3D Hall-Effect Magnetometer Using a Single Inverted Pyramid Structure

Ruggeri, Jacopo ; Strube, Jannik ; Dowling, Karen M.

DOI
10.1109/MEMS58180.2024.10439529

Publication date
2024

Document Version
Final published version

Published in
Proceedings of the 2024 IEEE 37th International Conference on Micro Electro Mechanical Systems (MEMS)

3D HALL-EFFECT MAGNETOMETER USING A SINGLE INVERTED PYRAMID STRUCTURE

Jacopo Ruggeri, Jannik Strube, and Karen M. Dowling*
Electronic Instrumentation Laboratory (EI), Department of Microelectronics,
Delft University of Technology, The Netherlands

2024 IEEE 37th International Conference on Micro Electro Mechanical Systems (MEMS) | 979-8-3503-5792-9/24/$31.00 ©2024 IEEE | DOI: 10.1109/MEMS58180.2024.10439529

ABSTRACT

This paper reports on the creation of a novel 3D Hall-effect sensor based on an anisotropically etched, inverted pyramid structure. Specific biasing and sensing contact configurations are employed to extract the in-plane or out-of-plane components of the magnetic field, eliminating cross-sensitivity by symmetry. Simulations were performed to verify the functionality and performance of the device, and the results suggested that sensitivity can be manipulated by varying the size-to-contact ratio. MEMS and CMOS processes were leveraged to create small-footprint, single-structure magnetometers with high in-plane/out-of-plane sensitivity. Four different geometries were characterized and maximum in-plane sensitivities of 80.1 V/A/T and 22.3 mV/V/T and in-plane to out-of-plane sensitivity ratios of up to 0.77/1.09 (current/voltage-related) were measured. The presented pyramid structure enables a path toward CMOS-integrated, spatially isotropic magnetometers using a single Hall sensor.

KEYWORDS

3D Magnetometer, Hall-Effect, Inverted Pyramid

INTRODUCTION

Hall-effect sensors are a cornerstone of automotive, industrial, and consumer electronics, holding the largest share of the magnetic sensor market (which is projected to reach $4.5 billion by 2028) [1]. Among them, silicon-based Hall sensors are particularly popular due to their high sensitivity and ease of integration with CMOS electronics [2], which enables the elegant fabrication of Hall devices and their readout circuits in the same technological process.

Hall-effect sensors come in two primary typologies: planar and vertical. Planar Hall devices (PHD) detect out-of-plane magnetic fields [3], while vertical Hall devices (VHD) detect in-plane magnetic fields [4]. 3D magnetic sensing with Hall sensors can be obtained by integrating, on the same platform, a PHD with two VHDs. However, the performance of such sensors is limited by the poor sensitivity and high offset of VHDs, respectively caused by the low junction depth available in modern CMOS technologies and the two-fold geometry of standard VHDs [5, 6]. Alternative solutions can be found in literature, such as the planar eight-contact structure proposed by Schott [7]. This concept reaches good sensitivity and low offset but still requires deep junction depths to properly operate. Another approach consists in adopting integrated magneto-concentrators to convert in-plane magnetic fields into out-of-plane fields, that are then detected by PHDs [8, 9, 10]. This solution solves the problems related to VHDs, but the presence of ferromagnetic materials increases packaging complexity, calibration, and post-processing costs. In addition, true isotropic detection cannot be achieved with any of the previous configurations since this feature requires either independently tuned 1D devices [11] or symmetrical 3D structures. 3D hexagonal Hall devices, as proposed by Sanders et al., manage to reach isotropic sensitivities due to their highly symmetric structure, but their complex manufacturing limits the integration into a standard CMOS process. [12]

In this paper, we propose a new type of single-structure 3D Hall sensor, realized with standard MEMS-manufacturing techniques and CMOS technological processes. The device reaches high sensitivities, both for in-plane and out-of-plane magnetic fields. This novel design reaches optimal performance with shallow active layers, enabling potential integration with modern CMOS technologies. In the following sections, we introduce the sensor concept along with initial simulation results, we illustrate the fabrication flow, and present and discuss the characterization data of the first-generation devices.

SENSOR DESIGN AND SIMULATION

3D Sensing Concept

The device is an inverted pyramid produced by TMAH anisotropic etching of silicon (100), exposing the (111) crystallographic planes with a characteristic angle of 54.74°. The sloped sidewalls are doped to define the active area of the device, which is contacted at the four corners and in the centers of the four sides.

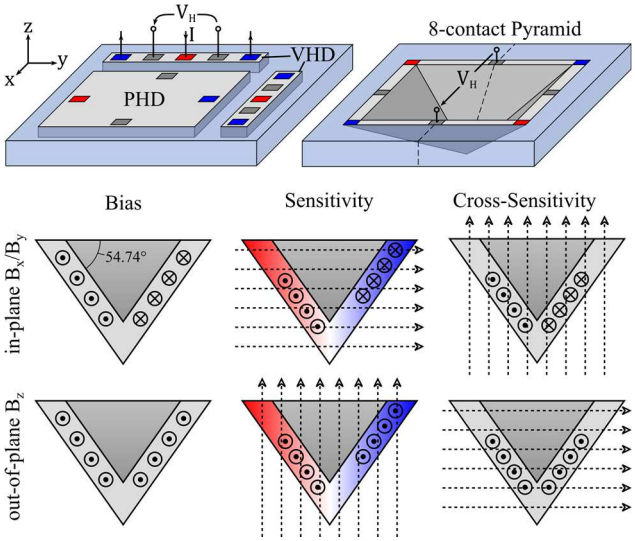

Figure 1: Top: Comparison of typical 3D Hall devices with pyramid concept. Bottom: In-plane and out-of-plane detection by controlling direction of current in pyramid sidewalls.

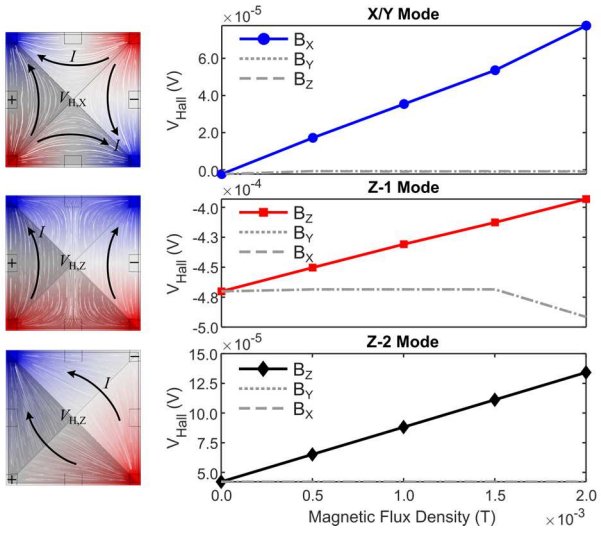

Figure 2: COMSOL simulation examples of a 50 µm wide pyramid in three different sensing modes (X/Y, Z-1, Z-2). Cross-sensitivity Z-1 curve affected by meshing errors.

The working principle of the device is illustrated in Figure 1. The sloped surfaces can be visualized as inclined triangular Hall plates, with one sense contact in the midpoint of the base sides and the other at the apex of the pyramid. The biasing contacts are placed at the base corners. To better understand the sensor concept, let us consider a single face of the device. The two components of the magnetic field, non-parallel to the biasing current, produce a Lorentz force that pushes the charge carriers either toward the top (base) or the bottom (apex) of the pyramid. This generates a Hall voltage difference between the two sense contacts of the sloped, triangular Hall plate. Due to the superposition principle, the overall Hall voltage will be a linear combination of the Hall voltages produced by each component of the magnetic field. This implies that each face is sensitive to the cross-plane magnetic field (B_z) and one component of the in-plane field (either B_x or B_y).

To distinguish the components of the magnetic field, specific biasing and sensing contact configurations on opposite faces are employed. The contact configuration is chosen so the desired component to be detected produces an accumulation of carriers on the top of one face, and a depletion on the opposite one, generating a measurable Hall voltage difference. The orthogonal component, instead, must produce an accumulation/depletion of carriers on the top of both faces, implying no Hall voltage difference. Such structure is then sensitive to only one component of the magnetic field, while the cross-sensitivity is removed by symmetry. Specifically, an anti-parallel biasing currents configuration is used to detect B_x and B_y, while a parallel biasing currents configuration is adopted to detect B_z (see Figure 1, 2). Since the pyramid structure presents two pairs of opposite, orthogonal faces, both the x- and y-component can be detected at the same time.

The theoretical in-plane and out of-plane absolute sensitivities have been extracted for the simplified case of a long v-groove:

$$S_A^z = 2\frac{r_h I_{bias}}{nqt}\cos\theta \qquad (1)$$

$$S_A^{x,y} = 2\frac{r_h I_{bias}}{nqt}\sin\theta \qquad (2)$$

where r_h is the Hall scattering coefficient, n is the majority carrier density, q is the elementary charge, t is the junction depth and θ is the etching angle (here $\theta = 54.74°$). Normalizing this result by the input voltage or current, voltage- (S_V) and current-related (S_I) sensitivities can be obtained. Like PHDs, the pyramid device's sensitivities benefit from shallow junction depths, opening a path toward integration with standard CMOS technologies [13].

3D Magnetic Sensor Simulation

The functionality and performance of the sensor were evaluated with FEM simulations (COMSOL). The study was simplified to an electrical conduction problem in a silicon pyramidal shell, and the conductivity tensor was explicitly defined to introduce the magnetic-field dependent terms. The tensor coefficients were extracted from the galvanomagnetic current equation [13]:

$$\boldsymbol{J} = \frac{\sigma}{(1+\mu_h B)^2}[\boldsymbol{E} + \mu_h(\boldsymbol{E}\times\boldsymbol{B}) + \mu_h^2\boldsymbol{B}(\boldsymbol{E}\cdot\boldsymbol{B})] \qquad (3)$$

where σ is the conductivity and μ_h is the Hall mobility. A constant electron mobility, uniform doping density and an abrupt junction with no depletion region influence were assumed for this analysis.

This model is able to reproduce the device's linear response to the applied magnetic fields with first order approximations, but it exhibits some minor meshing errors which cause small cross-sensitivity and offset artifacts in certain configurations (Figure 2). Three working modes were analysed, and the biasing and sensing contact configurations of each mode, as well as some examples of output curves for a 50 µm device (t = 1 µm, μ_h = 867 cm²/V/s and σ = 813.01 S/m), are displayed in Figure 2. Among these modes, X/Y detects B_x and B_y (where the Y-mode is identical to X-mode but rotated 90°), while Z-1 and Z-2 detect B_z.

Simulations were performed for various pyramid sizes and contact dimensions (features annotated in SEM image of Figure 4), with t = 2.5 µm, μ_h = 1212 cm²/V/s and σ = 188.54 S/m. The results suggest constant sensitivity for fixed size-to-contact ratio s/b, independent on the absolute dimensions of the pyramid cavity. The simulation results,

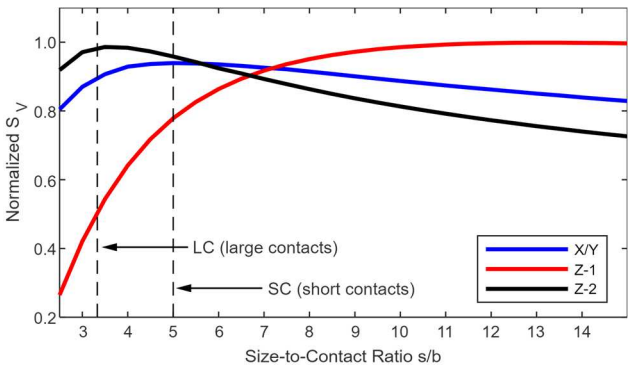

Figure 3: FEM simulation of voltage-related sensitivity dependent on pyramid size-to-contact ratio.

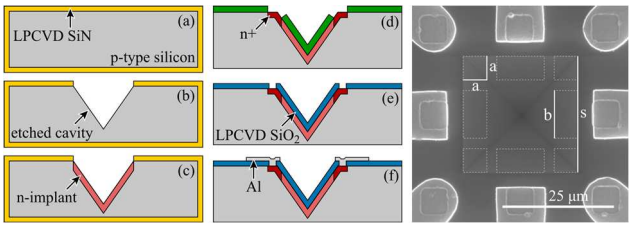

Figure 4: Left: Manufacturing process flow: (a) hard mask deposition (b) TMAH etching (c) active area n-implantation with phosphorus (d) contact n^+-implantation with arsenic (e) passivation and via opening (f) metallization. Right: SEM photograph of sensor 25-SC with geometry features labeled.

as displayed in Figure 3, indicate that the S_V of each mode can be manipulated by varying the size-to-contact ratio s/b. In addition, the graph features some s/b ratios for which the X/Y S_V is equal to Z-1 or Z-2 S_V. Isotropic detection can be then achieved, by tuning the geometrical proportions of the device ($5 < s/b < 7$).

FABRICATION

The fabrication process followed typical CMOS process steps, with some modifications with MEMS micromachining [14]. The process included pre-processing steps to produce the pyramid structures and the adoption of spray coating to conformally cover the sloped (111) surfaces. For comparison purposes, flat reference devices were also produced, that went through identical CMOS-based processing, but without anisotropic etching.

First, 500 nm-thick low-pressure chemical vapor-deposited (LPCVD) silicon nitride (SiH_2Cl_2 340 sccm; NH_3 60 sccm; 850 °C) was deposited onto the boron-doped (resistivity: 1 – 5 Ω·cm) (100) silicon wafer (Figure 4a). The nitride layer was patterned by reactive ion etching (RIE) with C_2F_6, and then the substrate was wet etched with TMAH 25 % at 90 °C (Figure 4b). The exposed sloped walls were implanted with phosphorous (100 keV; 4.5×10^{12} cm^{-2}) to define the active area of the device, re-using the silicon nitride layer as implantation mask (Figure 4c). After the silicon nitride wet removal and annealing at 1150 °C for 60 min, photoresist was spray-coated and patterned to define the n^+-contact regions, implanted with arsenic (40 keV; 5×10^{15} cm^{-2}) (Figure 4d). The photoresist was stripped, and 500 nm-thick LPCVD TEOS-based silicon oxide was deposited (TEOS bubbler 50 °C; 250 mTorr; 700 °C), annealed at 1000 °C for 30 min, and patterned to define the n^+-contact openings in the passivation layer (Figure 4e). Aluminum-silicon (1 %) was sputtered on the wafer at 350 °C (500 nm), and wet-etched to define the metal interconnections and pads (Figure 4f). The metal lines were annealed at 400 °C in a reducing atmosphere (N_2 3.0 L/min, H_2 0.2 L/min).

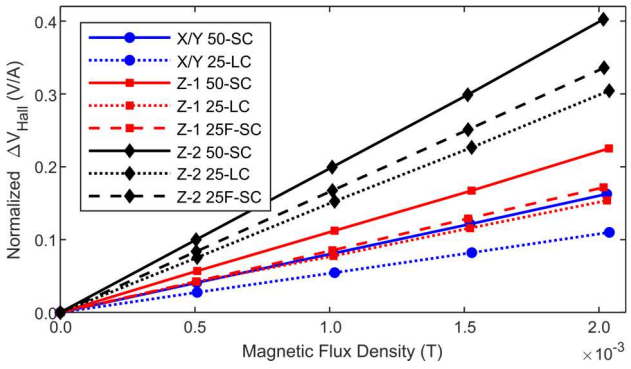

Figure 5: Normalized change in Hall voltage for sensors 50-SC, 25-LC, R-SC at 100 µA bias.

MEASUREMENT RESULTS

The fabricated devices were glued to a PCB and wire-bonded. Two different cavity sizes (25 µm and 50 µm) and size-to-contact ratios (large contacts LC: s/b = 3.33 and small contacts SC: s/b = 5) were selected for preliminary characterization. A planar reference Hall device (25F-SC) with no sloped walls was also wire-bonded and tested for comparison.

The electrical characterization was performed using a Keithley 2400 sourcemeter for bias, and an Agilent 34401A multimeter to measure the Hall voltage. The magnetic field was produced with a Helmholtz coil, with a range of 0 – 2 mT. The Hall voltage was measured in steps of 0.5 mT and averaged over 100 repeated measurements, to average out noise. The sensitivities of the devices were calculated at two bias currents: 50 and 100 µA.

The results are reported in Table I, and compared with state-of-the-art 3D Hall sensors [7, 12, 15]. Figure 5 depicts the normalized Hall voltage output of two sensors in three modes, compared to the flat reference device.

DISCUSSION

The highest achieved S_I ratio between Z-1 and X/Y mode is 0.77, measured for the 25-LC device. The overall highest in-plane S_I was obtained for the 50-LC sensor, with a value of 80.1 V/A/T. Mode Z-2 exhibits the highest S_I among the various configurations, probably because the biasing current is injected into one pair of contacts instead of two. The S_V vary from 18.0 – 23.5 mV/V/T and are

Table 1: Sensitivity of tested pyramid 3D Hall sensors compared with prior art 3D Hall sensors.

Sensor*	Dimensions (µm)	S_V (mV/V/T)				S_I (V/A/T)			
	s/a/b	X/Y	Z-1	Z-2	$S_{X/Y}/S_Z$	X/Y	Z-1	Z-2	$S_{X/Y}/S_Z$
50-SC	50/5/10	21.8	23.5	21.3	0.93 – 1.02	80.1	109.8	198.2	0.40 – 0.73
50-LC	50/7.5/15	19.6	18.4	18	1.07 – 1.09	39.3	56.4	110.7	0.36 – 0.70
25-SC	25/2.5/5	22.3	22.9	20.6	0.97 – 1.08	79.6	103.4	188.7	0.42 – 0.77
25-LC	25/3.75/7.5	20.2	20.6	20.7	0.98	53.3	73.9	148	0.36 – 0.72
25F-SC	25/2.5/5	-	35.7	34.6	-	-	85.1	166.3	-
[15]	PHD + VHD	-	-	-	-	6.19	84.25	-	0.07
[7]	PHD 8-contact	20 – 54	20 – 33	-	0.95 – 2.70	46 – 827	17 – 909	-	0.91 – 2.71
[12]	hex. prism	19.7	20.2	-	0.96	-	-	-	-

*SC small contacts, LC large contacts

isotropic within 9 % for in-plane/out-of-plane modes. The inverted-pyramid sensors present a 6 to 12 times higher in-plane S_I than a PHD + VHD sensor, and both 25-SC and 50-SC devices show also a higher out-of-plane S_I. The S_V in-plane/out-of-plane isotropy displayed is comparable with the hexagonal prism 3D Hall sensors, and even superior for 50-SC and 25-LC. The characterized devices did not achieve the sensitivities reported for the 8-contacts PHD (54 mV/V/T and 827 V/A/T for X/Y), but future designs with optimized geometrical features, junction depths and doping might be able to partially bridge the gap.

Compared to the planar 25F-SC, the corresponding pyramid (25-SC) had a 36 % and 40 % reduction in S_V, respectively for Z-1 and Z-2 modes. However, the S_I increased 13 % for Z-2 and 21 % for Z-1. We attribute this effect to the change in geometry and increase in input resistance. It will be further investigated in future work.

There is a noticeable discrepancy between experimental and simulation results. The measured S_V do not line up with the trends represented in Figure 3, which is likely due to fabrication inaccuracies. Some probable causes are imprecise lithographic transfers during the patterning of the spray-coated photoresist, as well as differences from the nominal pyramid size due to TMAH undercut. On the other hand, it is possible that the simulation model does not precisely represent the fabricated devices. In fact, it cannot be excluded that the trend displayed in Figure 3 depends on parameters such as doping and junction depth, which differ between simulations and experimental results.

Finally, raw offsets have been extracted for 10 – 100 µA bias in all devices, ranging from 220 µT – 390 mT. The origin of the high offset is still under investigation, but it might be due to asymmetries in the patterning of spray-coated photoresist, or doping inhomogeneity, in addition to design challenges similar to VHDs [6]. Offset and the simulation-experimental data discrepancy will be analyzed in future work.

CONCLUSIONS

This paper introduced a novel 3D Hall-effect sensor design based on an inverted pyramid structure. Utilizing MEMS and CMOS processes, monolithic magnetometers were successfully manufactured with high sensitivity to both in-plane and out-of-plane magnetic fields. The devices displayed a maximum in-plane S_I of 80.1 V/A/T, which is around twelve times higher than CMOS-integrated VHD-based 3D magnetic sensors. The measured S_V are in the range 18.0 mV/V/T – 23.5 mV/V/T, in line with state-of-the art Hall devices, and present isotropy comparable or superior to alternative sensor concepts. Some challenges, such as high offsets, are present, but nonetheless this device is a promising candidate for the new generation of CMOS-integrated, spatially isotropic 3D magnetometers.

ACKNOWLEDGMENTS

This work was supported in part by the Delft Technology Fellowship, the Nanotech for ICTs MSc program, and the TU Delft Microelectronics Department. The authors would like to thank the Else Koi Laboratory (EKL) team for their fabrication support, especially Paolo Sberna, Francesco Stallone, Daniel van der Plaats and Henk van Zeijl. We also thank Zu Yao Chang, Ron van Puffelen, and Lukasz Pakula for their lab testing support, Massimo Mastrangeli for the advice on fabrication, and Jiarui Mo. A special thanks to Infineon Technologies for the interest in the project, in particular to Helmut Köck, Udo Ausserlechner and Steffen Rothenhaeusser.

REFERENCES

[1] S. Leroy, Leroy Group, https://www.yolegroup.com/strategy-insights/a-new-milestone-in-the-tmr-industry/ [accessed 25 October 2023].

[2] A. Karsenty, "A comprehensive review of Integrated Hall effects in macro-, Micro-, Nanoscales, and quantum devices", *Sensors*, vol. 20(15):4163, 2020.

[3] C. Roumenin, P. Kostov, "Planar Hall-effect device", Bulgarian Patent 37.208(1983):26.

[4] R.S. Popović, "The vertical hall-effect device". *IEEE Electron Device Letters,* vol. 5(9), 1984, pp. 357–358.

[5] J. Pascal, L. Hébrard, V. Frick, J.-B. Kammerer, J.-P. Blondé, "Intrinsic limits of the sensitivity of CMOS integrated vertical hall devices", *Sensors and Actuators A: Physical,* vol. 152(1), 2009, pp. 21–28.

[6] O. Paul, R. Raz, T. Kaufmann, "Analysis of the offset of semiconductor vertical hall devices", *Sensors and Actuators A: Physical,* vol. 174, 2012, pp. 24–32.

[7] Ch. Schott, J.-M Waser, R.S. Popović, "Single-chip 3-D silicon hall sensor", *Sensors and Actuators A: Physical,* vol. 82(1–3), 2000, pp. 167–173.

[8] R.S. Popović, P. Drljača, Ch. Schott, R. Racz, "A new CMOS Hall angular position sensor", *Technisches Messen,* vol. 68(6), 2001, p. 286-291.

[9] R.S. Popović, P.M. Drljača, Ch. Schott, R. Racz, "Integrated HALL sensor/flux concentrator microsystems", *Informacije MIDEM,* vol. 31(4), 2001, pp. 215–219.

[10] R. S. Popović, Ch. Schott, "Hall ASICs with Integrated Magnetic Concentrators", 2002.

[11] S. Guo, "Integrated three-dimensional hall switch sensor based on independent optimized hall devices", *Microelectronics Journal,* vol. 135:105756, 2023.

[12] C. Sander, C. Leube, T. Aftab, P. Ruther, O. Paul, "Monolithic isotropic 3D Silicon Hall sensor", *Sensors and Actuators A: Physical,* vol. 247, 2016, pp. 587–597.

[13] R. S. Popović, *Hall effect devices (Series in Sensors), 2nd edition*, CRC Press, 2003.

[14] Z. Kolahdouz Esfahani, "Monolithic 3D Wafer Level Integration: Applied for Smart LED Wafer Level Packaging", Dissertation (TU Delft), Delft University of Technology, 2017.

[15] J.-B. Schell, J.-B. Kammerer, L. Hébrard, E. Breton, D. Gounot, L. Cuvillon, M. de Mathelin, "CMOS 3D Hall probe for magnetic field measurement in MRI scanner", *10th IEEE International NEWCAS Conference*, Montreal, 17-20 June, 2012, pp. 517-520.

CONTACT

*J. Ruggeri, email: j.ruggeri@tudelft.nl